Batteries & Supercaps

Research Article
doi.org/10.1002/batt.202300164

Chemistry Europe
European Chemical Societies Publishing

www.batteries-supercaps.org

Special Collection

Hydride-Enhanced Plating and Stripping of Aluminum from Triflate-based Organic Electrolytes**

Zaher Slim[a, b] and Erik J. Menke*[a]

In the quest for developing rechargeable aluminum (Al) batteries, reversible Al plating in the absence of active-halide components is considered an immense challenge. For this reason, the choice of electrolyte has been primarily limited to the highly corrosive chloroaluminate systems based on aluminum trichloride ($AlCl_3$). In this work, we demonstrate reversible room-temperature Al plating from an active-halide-free (AHF) organic electrolyte based on aluminum trifluoromethanesulfonate ($Al(OTF)_3$) and lithium aluminum hydride ($LiAlH_4$) in tetrahydrofuran (THF), as well as its $AlCl_3$ counterpart. From insights obtained by Density Functional Theory (DFT) and Fourier-Transform Infrared (FTIR) spectroscopy, ionic speciation in the electrolyte is explored, and mechanisms for the underlying electrochemical processes in the trifluoromethanesulfonate (OTF^-)-based electrolytes are proposed. Al plating and stripping were confirmed by optical microscopy, scanning electron microscopy (SEM) and X-ray diffraction (XRD). Characterizing the Al deposits from either the OTF^-- or the chloride (Cl^-)-based electrolytes via depth-profile X-ray Photoelectron Spectroscopy (XPS) analyses, we find that these deposits consist of metallic Al, aluminum oxide (Al_2O_3), and either aluminum trifluoride (AlF_3) or aluminum chloride (Al_xCl_y) contaminants arising from a reaction with the electrolyte components which occurs during the plating process.

Introduction

The promise of an energy sustainable society – that is, a society whose primary energy is derived from inexhaustible energy resources (such as, wind, water, and solar radiation) calls for major advances in materials for energy storage devices (such as, rechargeable batteries and electrochemical capacitors).[1] Notable example of energy storage devices are lithium (Li)-ion batteries, which have dominated the global battery market.[2–4] While these batteries have undoubtedly revolutionized modern society's living standards, it is highly unlikely that Li-based technology can solely meet future demands for energy storage devices. As a result, global research efforts in pursuit of alternative battery chemistries that utilize earth-abundant materials such as, sodium (Na), magnesium (Mg), calcium (Ca), and aluminum (Al), have amplified.[4,5]

The rechargeable Al battery is a likely candidate for next-generation energy storage systems due to Al's unmatched theoretical volumetric capacity (8046 mAh/cm^3 compared to 2042 mAh/cm^3 for Li), abundant resources (82000 ppm compared to 65 ppm for Li), and considerably low cost (1.9 USD/kg compared to 19.2 USD/kg for Li).[6] Very few electrolytes are capable of plating/stripping Al,[7,8] and most research on rechargeable Al batteries employ chloroaluminate ionic liquids as the electrolyte.[9–19] These systems typically consist of aluminum trichloride ($AlCl_3$) and 1-ethyl-3-methyl imidazolium chloride (EMIMCl). Depending on the mole ratio (r) of $AlCl_3$ to EMIMCl, these mixtures are often divided into 3 types: basic ($r<1$), neutral ($r=1$), and acidic ($r>1$) melts.[7,20,21] Furthermore, reversible Al plating and stripping, which is an essential criterion for realizing rechargeable Al batteries, can only be achieved from acidic ionic liquids due to the presence of both $Al_2Cl_7^-$ and $AlCl_4^-$ complexes. It is important to note that the electrochemical reaction at the anode is dictated by both complexes, and that the formation of such species necessitates the presence of free Cl^-.[7,20–22] Counterintuitively, chloroaluminate ionic liquids are especially problematic for practical application due to the active-halide components – that is $Al_2Cl_7^-$, $AlCl_4^-$ and free Cl^-.[11,19,23] While these systems demonstrate impressive cycleability with certain cathode materials,[14–18] they suffer from high corrosivity and reactivity towards battery components,[11,19,24,25] and side reactions involving toxic chlorine (Cl_2).[26,27]

One approach to overcome these challenges is through the development of active-halide-free (AHF), or as commonly referred to, chloride-free organic electrolytes.[23] AHF electrolytes take advantage of the fact that the halogen atoms are sequestered in a polyatomic anion,[28] which renders these systems free from the intrinsically corrosive haloaluminate complexes (for example, $Al_2Cl_7^-$, $AlCl_4^-$, and solvated $AlCl_3$) and free halide anions (for example, F^-, Br^- and Cl^-). One such example of these polyatomic anions is the trifluoromethanesulfonate anion (OTF^-), which is known to be exceptionally stable

[a] Dr. Z. Slim, Prof. Dr. E. J. Menke
Department of Chemistry & Biochemistry
University of California, Merced
95343 Merced, California (USA)
E-mail: emenke@ucmerced.edu

[b] Dr. Z. Slim
Department of Physics
Chalmers University of Technology
41296 Göteborg (Sweden)

[**] A previous version of this manuscript has been deposited on a preprint server (DOI: https://doi.org/10.26434/chemrxiv-2022-sv3gn-v4)

Supporting information for this article is available on the WWW under https://doi.org/10.1002/batt.202300164

Special Collection An invited contribution to a Special Collection dedicated to NordBatt 2022 conference.

to both oxidative and reductive cleavage,[29] thus, making OTF^--electrolytes suitable candidates for AHF systems and of potential application in rechargeable Mg[30–32] and Al batteries.[33,34]

Thus far, only a handful of AHF organic electrolytes for rechargeable Al batteries have been reported.[33,35–41] A timeline showing the progress in chloride-based[42–67] and AHF organic electrolyte development is shown in Figure S1. Early work on AHF electrolytes involved aluminum trifluoromethanulfonate ($Al(OTF)_3$) and urea in N-methyl acetamide (NMA),[36] and $Al(OTF)_3$ in 2-methoxy ethyl ether (diglyme).[33,35] Unfortunately, from both systems, Al plating could not be carried out. Following their work on $Al(OTF)_3$ and urea in NMA, Mandai and Johansson introduced an interesting strategy for the development of AHF electrolytes.[37] Several promising electrolyte systems were reported, including aluminum *hexa*-dimethylsulfoxide trifluoromethanesulfonate $[Al(DMSO)_6][OTF]_3$ in sulfolane, aluminum *hexa*-dimethyl sulfoxide bis(trifluoromethanesulfonyl)imide $[Al(DMSO)_6][TFSI]_3$ in sulfolane, aluminum *hexa*-methylimidazole bis(trifluoromethanesulfonyl)imide $[Al(MIm)_6][TFSI]_3$ in acetonitrile (MeCN), and aluminum *hexa*-butylimidazole bis(trifluoromethanesulfonyl)imide $[Al(BIm)_6][TFSI]_3$. Al plating was attempted from $[Al(BIm)_6][TFSI]_3$ at 80 °C, however, the Al plating process was accompanied by severe electrolyte decomposition.

While considerable progress has been made, only two systems have shown promising reversible Al electrochemistry. Notable work on the synthesis of $Al(TFSI)_3$ and aluminum hexafluorophosphate ($Al(PF_6)_3$) salts was conducted by Chiku et al.[38] and Wen et al.,[40] respectively. Although evidence for Al plating was reported for the $Al(TFSI)_3$/MeCn electrolyte, the demonstrated reversibility of this process was unclear, and therefore requires further investigation.[38] On the other hand, quasi-reversible Al plating/stripping along with a side reaction involving the reductive generation of dimethyl sulfide was demonstrated from $Al(PF_6)_3$/DMSO. Surprisingly, however, the Al plating and stripping potentials were of unusually low-energy efficiency, with a reduction and oxidation potentials of −1 V and + 0.5 V (vs. Al/Al^{3+}), respectively.[40]

In comparison with the $Al(TFSI)_3$ and $Al(PF_6)_3$ salts, $Al(OTF)_3$ is commercially available, and as mentioned earlier, Reed et al. investigated this salt in diglyme. Although Al plating from the $Al(OTF)_3$/diglyme was not achieved,[35] reversible intercalation/deintercalation behavior was demonstrated with a Prussian blue analogue cathode.[33] Unlike the $Al(OTF)_3$/diglyme electrolyte, however, non-reversible Al plating can be carried out from $Al(OTF)_3$ in tetrahydrofuran (THF) electrolytes, as we have revealed in our previous reports.[39,41]

To highlight the role of hydrides (H^-) in the Al plating/stripping process, in this report, we demonstrate reversible Al plating/stripping from an AHF organic electrolyte based on $Al(OTF)_3$/THF facilitated by a lithium aluminum hydride ($LiAlH_4$) additive. The spectroscopic and electrochemical aspects of the trifluoromethanesulfonate (OTF^-)-based electrolyte were evaluated and compared to the well-known chloride (Cl^-)-based system.[42,45,46,48–50,55–57,68] This comparison revealed that the H^- species not only catalyzes the Al plating/stripping process in the Cl^--based electrolytes as previously proposed by Daenen[68] and Graef,[49] but also allows for this process to be carried out in the absence of any haloaluminate species (such as, $AlCl_2^+ \cdot n$THF, $AlCl_3 \cdot n$THF and $AlCl_4^-$ where n = number of coordinating THF).

Density functional theory (DFT) calculations along with Fourier transform infrared spectroscopy (FTIR) analyses reveal remarkably dissimilar Al-hydride speciation in these two systems. Unambiguous evidence for Al plating and stripping is demonstrated using an optical microscope, a scanning electron microscope (SEM) and X-ray diffraction (XRD). Characterization by means of X-ray photoelectron spectroscopy (XPS) indicates that the deposits from the OTF^--based electrolyte comprise metallic Al, aluminum trifluoride (AlF_3) and aluminum oxide (Al_2O_3), whereas the deposits from the Cl^--based electrolyte comprise mainly aluminum chloride contaminants (Al_xCl_y) and Al_2O_3. Depth profile XPS analyses of the Al films from either the OTF^--based or the Cl^--based electrolytes suggest that during the plating process, freshly deposited Al reacts with the electrolyte components to form Al_2O_3 and either AlF_3 (from the OTF^--based) or $AlCl_3$ (from the Cl^--based).

Materials and Methods

Density functional theory calculations

All density functional theory (DFT) calculations were carried out using Gaussian 09 suite of electronic structure program.[69] Unless otherwise stated, the default settings for structure optimization and frequency calculations were used. All results were obtained using the unrestricted spin-formalism employing Becke's three parameter exchange functional with the Perdew and Wang correlation functional (B3PW91)[70] together with the 6311 + G(d) basis set.[71] All structures were fully optimized using standard techniques and carried out using the solvation model density (SMD) continuum solvation model based on the self-consistent reaction field (SCRF) approach, and THF ($\varepsilon = 7.42$) was used as the solvent for all calculations. All structures were found to be local minima on the potential energy surfaces by confirming the absence of any imaginary frequencies.

Electrolyte preparation

All chemical preparations were conducted in an argon-filled glovebox. 99.9% aluminum trifluoromethanesulfonate ($Al(OTF)_3$), 99.99% aluminum trichloride ($AlCl_3$), 97% lithium aluminum hydride ($LiAlH_4$), 99.9% tetrahydrofuran (THF), were all purchased from Sigma-Aldrich and used as received. To prepare the OTF-based electrolyte, a 1 : 3 mole ratio of $Al(OTF)_3$ to $LiAlH_4$ was used. Initially, 0.2 g of $LiAlH_4$ were dissolved in 3.5 mL of THF. Similarly, 0.83 g of $Al(OTF)_3$ were dissolved in 3.5 mL in THF. Both solutions were stirred separately for at least 30 minutes to ensure complete dissociation. The $LiAlH_4$/THF solution was slowly added drop-wise to the $Al(OTF)_3$/THF solution under moderate stirring. It should be noted that the reaction between the two solutions is extremely exothermic, and mixing the solutions should be carried out slowly, otherwise excessive solution foaming and THF evaporation may take place. The mixture was allowed to stir for 30 minutes. While Al plating can be carried out at this point, the excessive hydride activity due to the elevated temperature in the solutions can be

problematic. For this reason, the mixture was allowed to rest (without stirring) for several hours before measuring the oxidative stability of the electrolyte (see Figure S4). The chloride-based electrolytes were prepared according to the same procedures using appropriate amounts of $AlCl_3$ (0.23 g), to ensure the total concentration of [Al] is the same in both electrolytes. Both electrolytes used for the 4-hour chronoamperometry experiments contained the same total concentration of Al. As for the electrolyte used for the 18-hours chronoamperometry experiment, the concentration was higher, and the electrolyte consisted of 0.4 g of $LiAlH_4$ and 1.23 g of $Al(OTF)_3$ in 5 mL of THF. For the Cl^--based electrolyte a grey precipitate forms in as little as 15 minutes after the two solutions have been mixed, whereas for the OTF^--based electrolyte a precipitate forms several hours after preparation. Moderate stirring of the OTF^--based electrolyte for one minute is enough to redissolve the grey precipitate and regain typical electrochemical activity from this system.

Experimental details and characterization

All electrochemical measurements were conducted in an argon-filled glovebox using a potentiostat (Gamry). Cyclic voltammetry experiments were carried out using a standard three-electrode set up using a gold working electrode, an Al wire pseudo-reference, and an Al wire as the counter electrode. A 50 mV/s scan rate was used. Chronoamperometry experiments were carried out using a Cu substrate as the working electrode, an Al wire as a pseudo-reference, and an Al wire as the counter electrode. Immediately after the chronoamperometry experiments were done, the Cu substrates were rinsed with THF in the glovebox. Chronoamperometry for the 4 hours samples from both OTF^--based and the Cl^--based electrolytes were done by setting the potential to −0.25 V (vs. Al/Al^{3+}). For the 18 hour sample from the OTF^--based electrolyte, plating was conducted at −0.2 V (vs. Al/Al^{3+}) from a highly concentrated solution consisting of 0.4 g of $LiAlH_4$ and 1.23 g of $Al(OTF)_3$ in 5 mL of THF. Fourier Transform Infrared Spectroscopy (FTIR) experiments were done in attenuated total reflectance (ATR) mode using a Vertex 70 spectrometer. A 4 cm^{-1} resolution and 64 scans were used. X-ray photoelectron spectroscopy (XPS) measurements were carried out using a Nexsa spectrometer. Etching experiments were conducted using argon at a rate of 0.9 nm/sec. In all cases, 5 scans were collected. No pretreatment or peak calibration was done for the XPS spectra. X-ray Diffraction (XRD) measurements were carried out using a Panalytical X'Pert PRO X-ray diffractometer, using a Co-K_α source. The spectra were then converted to Cu-K_α source using the HighScore software. The sample holders for the XRD were filled with polyethylene glycol (PEG) and the Cu substrates were laid on top of the PEG. Electron microscopy experiments were conducted using a field emission Scanning Electron Microscope (Zeiss Gemini SEM 500) and optical microscopy images were obtained using an ECLIPSE LV150 A microscope.

Results and Discussion

Exploring Ionic speciation using DFT and FTIR

The electrolytes were prepared by slowly adding a solution of $LiAlH_4$/THF to a solution of either $AlCl_3$/THF or $Al(OTF)_3$/THF. Identifying the Al species that are likely to be found in the studied electrolytes is crucial to elucidate the electrochemical mechanism for reversibly plating and stripping of Al from the OTF^--based electrolyte. DFT calculations for several Al complexes were performed and the optimized structures are shown in Figure 1(A–F. A summary of the calculated vibrational frequencies can be found in Table S1 in the Supporting Information. To experimentally substantiate the existence of such species, FTIR spectra for four electrolyte solutions were collected, and different regions of the spectra are shown in Figure 1(G–L). Motivated by the exceptional work conducted by Frech et al.[72,73] on the spectroscopic attributes of the OTF^-, in our previous work on $Al(OTF)_3$/THF we described a new method that allows for the determination of the reaction progress between $Al(OTF)_3$ and Li-based salts by exploiting the computed and measured spectroscopic features of the OTF^-.[41] Indeed, these results are well represented by the FTIR measurements shown in Figure 1(G). Upon the addition of $LiAlH_4$ to the $Al(OTF)_3$/THF electrolyte at 1:3 mole ratio, a shift in frequency from 1238 to 1253 cm^{-1}, corresponding to the transfer of the OTF^- from Al to Li ions, is observed. Additionally, the peak at 1350 cm^{-1} associated with the presence of Al-OTF aggregates (Al-Agg) disappears, further indicating that the OTF^- are no longer associated with Al ions.

FTIR spectra for the Cl^--based electrolytes shown in Figure 1(H and I) reveal that the bands associated with $AlCl_3$(THF), cis- and trans-$AlCl_3(THF)_2$, those previously identified in an $AlCl_3$/THF solution,[41,74] remain intact. However, peaks attributable to a new species are observed at 501 and 667 cm^{-1}. Our DFT calculations suggest that these peaks are associated with the asymmetric stretch (ν_{as}(Al–Cl)) and AlH_3 group bending (δAlH_3) of $Al_2Cl_3H_4^-$, respectively. Moreover, the ν_{as}(Al–Cl) band for $AlCl_3(THF)_2$ was measured at 490 cm^{-1} in the $AlCl_3$/THF electrolyte.[41,74] The shift in frequency for the ν_{as}(Al–Cl) mode from 490 to 501 cm^{-1} suggest that strong ionic association is taking place. It is important to note that the presence of $AlCl_3H^-$ in a H^- rich environment was confirmed by the detailed NMR studies conducted by Lefebvre and Conway,[55] however, computational and experimental evidence for the ionic association of $AlCl_3H^-$ with AlH_3 is presented here for the first time. Next, we examine the region associated with the hydride species. Inspecting the $LiAlH_4$ spectra (i) in Figure 1(J), one can clearly see two adjoint peaks at 1645 and 1668 cm^{-1}. Our DFT calculations suggest that these bands are attributed to the Al–H asymmetric stretch (ν_{as}(Al–H)) of the $LiAlH_4$ and AlH_4^- species, respectively (see Table S1). It should be noted that the ν_{as}(Al–H) mode involves all 4 hydrogen atoms.

In the OTF^--based electrolyte, however, the peak associated with $LiAlH_4$ disappears. These results are also consistent with the fact that the Li ions in the OTF^--based electrolyte are associated with the OTF^-, weakening the interaction between Li and AlH_4^-, thus, resulting in free AlH_4^- species, which dominates the ionic profile of the OTF^--based electrolyte. Comparatively, the spectrum for the Cl^--based electrolyte shown in Figure 1(L) reveals several bands associated with three distinct Al-hydride complexes. According to our DFT calculations, the bands at 1711 and 1800 cm^{-1} are attributable to the $AlH_3(THF)_2$ and AlH_3(THF), respectively. Furthermore, DFT results for the $Al_2H_7^-$ suggests that this species exhibits two strong vibrational modes associated with ν_{as}(Al–H) at 1778 and 1800 cm^{-1}. These results suggest that the existence of a hydride bridge between two

Research Article
doi.org/10.1002/batt.202300164
Chemistry Europe
European Chemical Societies Publishing

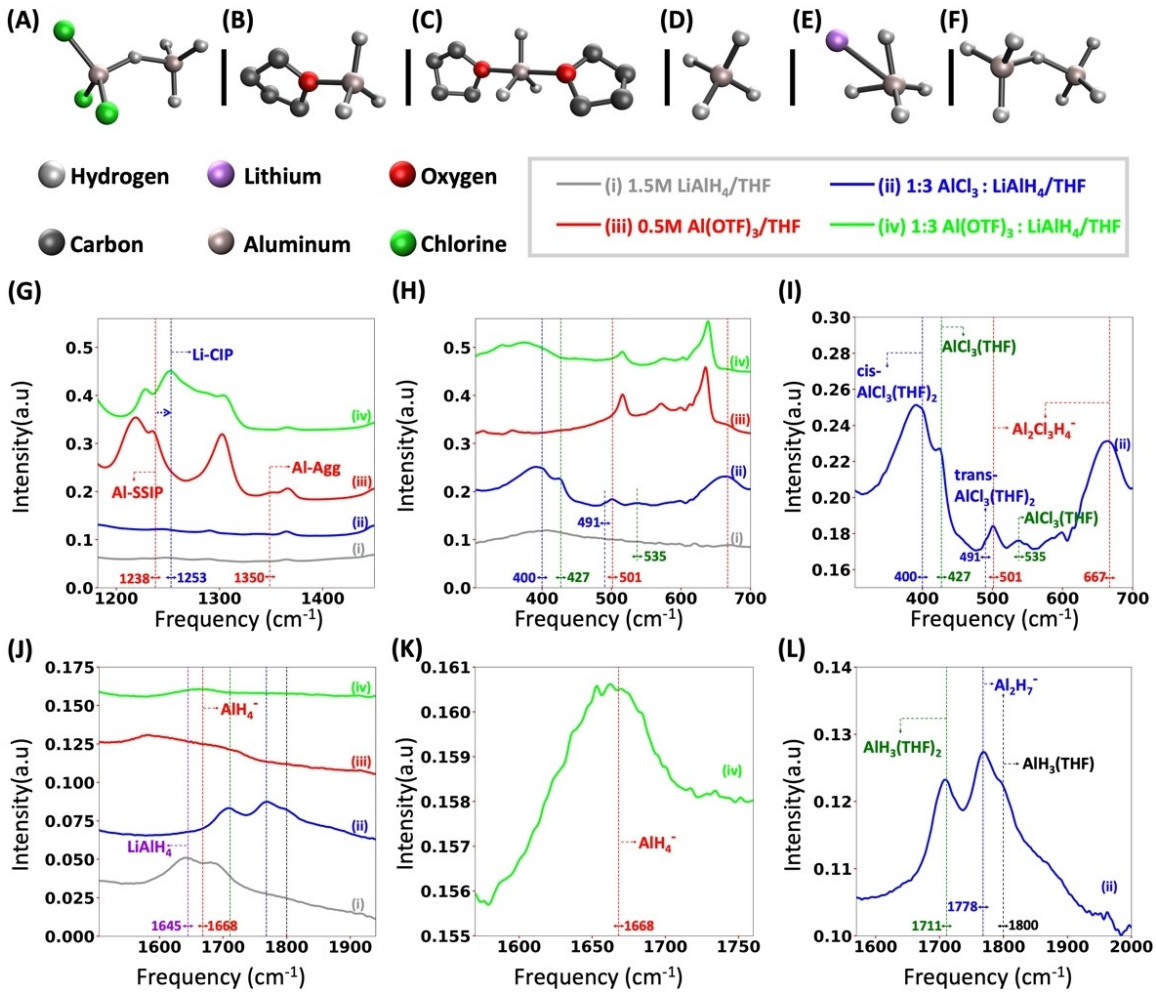

Figure 1. Optimized structures (hydrogens only shown for Al–H bonds) of various Al-complexes and FTIR spectra of various THF-based Al electrolytes. A) $Al_2Cl_3H_4^-$, B) $AlH_3(THF)$, C) $AlH_3(THF)_2$, D) AlH_4^-, E) $LiAlH_4$, F) $Al_2H_7^-$, G) $\nu_{as}SO_3$ shifting corresponding to OTF^- transfer from Al to Li ions, H) Al-chloride speciation region for all electrolyte solutions, I) Al-chloride speciation region for the Cl^--based electrolyte, J) Al-hydride speciation region, K) zoomed in Al –H stretching region for the OTF^--based electrolyte, L) zoomed in Al–H speciation region for the Cl^--based electrolyte. SSIP: solvent-separated ion pairs, CIP: contact ion pairs, Agg: aggregates. Please note that the hydride bridging depicted in structures (A) and (F) are the result of short range interactions between the $AlCl_3H^-$ and AlH_3, and AlH_4^- and AlH_3, respectively.

AlH_3 is likely to occur in the Cl^--based electrolytes, particularly because the calculated bond length between the bridging hydride and the AlH_3 is ca. 1.71 Å as shown in Figure S2, this bond length is equal to the bridging Al–H bond length reported for solid AlH_3.[75] Interestingly, these bands are absent from the OTF^--based electrolyte. Clearly, the ionic profiles of both systems are radically distinct. The discrepancy between the Al-hydride species in OTF^--based and Cl^--based electrolytes arises from the unique bonding profiles of $Al(OTF)_3$ in THF and $AlCl_3$ in THF. In the former, the coordination of Al with the OTF^- is relatively weak, which results in the presence of free OTF^-, contact ion pairs (CIP) and aggregates (Agg) upon dissolving $Al(OTF)_3$ in THF.[39,41] When a Li-based salt is added at 1:3 mole ratio's, complete transfer of the OTF^- from Al to Li ions occurs, as demonstrated in this work and our previous work.[41] As for the later, Cl^- are never completely detached from Al due to the strong and covalent nature of the Al–Cl bond,[37] which results in mixed speciation when $LiAlH_4$ is added to $AlCl_3$/THF solutions. Furthermore, the binding energies for Al^{3+}–OTF^-, Al^{3+}–Cl^- and Al^{3+}–H^- were calculated and found to be −970, −1085 and −1345 kJ/mol, respectively. (Table S2). These results further support that the interaction between Al^{3+}–OTF^- is much weaker than that of either Al^{3+}–Cl^- or Al^{3+}–H^-. It has been proposed that Al speciation in the Cl^--based electrolyte occurs according to the Schlesinger reaction (Reaction 1):[55,56,76]

$$AlCl_3 + AlH_4^- + 2THF \rightleftharpoons AlH_xCl_{(3-x)}(2THF) + [AlH_{(4-x)}Cl_x]^- \quad (1)$$

It is worth emphasizing that in the previous studies by Lefebvre and Conway, it was proposed that the high Lewis acidity of the $AlCl_3$ facilitates solution decompositions in the Cl^--based electrolytes.[55]

Based on these results, we propose the following dissociation reaction mechanism in the OTF^--based electrolytes at 1:3 mole ratio of $Al(OTF)_3$ to $LiAlH_4$ in THF (Reaction 2):

Research Article
doi.org/10.1002/batt.202300164
Chemistry Europe
European Chemical Societies Publishing

$$Al(OTF)_3 + 3LiAlH_4 \rightarrow 4AlH_3 + 3LiOTF \quad (2)$$

Evaluating the electrochemical behavior using cyclic voltammetry and chronoamperometry

The plating/stripping behavior of Al from the Cl^-- and the OTF^--based electrolytes were evaluated by cyclic voltammetry using a gold working electrode in a three-electrode electrochemical cell. Prior to mixing the $LiAlH_4$/THF with the $AlOTF_3$/THF solutions, it is essential to first record a cyclic voltammogram (CV) for the $LiAlH_4$/THF. The CV is shown in Figure S3. Our measurements are consistent with those of Lefebvre and Conway,[56] revealing a reversible electrochemical process between −1 and 0 V (vs. Al/Al^{3+}), likely associated with plating of Li and possibly the co-plating of Al. This is perhaps due to the strong interaction between Li ions and AlH_4^- as revealed by the above-mentioned DFT and FTIR results.

Figure 2(A) shows a typical CV for the 1:3 $Al(OTF)_3$:$LiAlH_4$/THF electrolytes. Upon sweeping to a more negative potential, a cathodic current is immediately measured ca. −0.2 V (vs. Al/Al^{3+}), and a CV typical to reversible electrochemical plating is recorded. On the reverse sweep, stripping of the deposited Al takes place ca. 0 V (vs. Al/Al^{3+}), with minimal plating/stripping potential hysteresis. Comparatively, the CV for the Cl^--based electrolyte shown in Figure 2(B) exhibits a similar profile, with the appearance of an Al nucleation loop during the negative potential sweep. In this electrolyte, however, oxidative decomposition occurs ca. +1.1 V (vs. Al/Al^{3+}), consistent with the measurements of Lefebvre and Conway.[56]

Furthermore, while recording the CVs for the OTF^--based electrolyte, an unusual feature in the CVs is observed ca. +1 V (vs. Al/Al^{3+}) (Figure S4A). This feature was investigated by sweeping the potential from 0 to +1.5 V (vs. Al/Al^{3+}), which is shown in Figure S4B. This oxidation reaction can be attributed to side reaction involving H_2 generation as shown in Reaction (4). It is worth noting that this feature is usually amplified within the first hour after the electrolyte has been prepared as shown in Figure S4 C and D, likely due to the elevated temperature of the solution which arises from the highly exothermic reaction between $Al(OTF)_3$ and $LiAlH_4$.

Moreover, the cycling behavior of the OTF^--based electrolytes was further evaluated on a gold electrode and is show in Figure 2(C). The corresponding coulombic efficiencies (the ratio of anodic charge to cathodic charge) are shown in Figure 2(F). Throughout the cycling process, a widening of the oxidative feature near 1 V (vs. Al/Al^{3+}) is observed, leading to a coulombic efficiency increase from ~60% to 80%. It should be noted that the stripping peak is likely a combination of both Al stripping and the side reaction involving H_2 generation. According to these results, we propose the following electrochemical reaction mechanisms at 1:3 mole ratio of $Al(OTF)_3$ to $LiAlH_4$ in THF:

$$4AlH_3 + 3e^- \rightleftharpoons Al + 3AlH_4^- \quad (3)$$

$$2AlH_4^- \rightarrow 2AlH_3 + H_2 + 2e^- \quad (4)$$

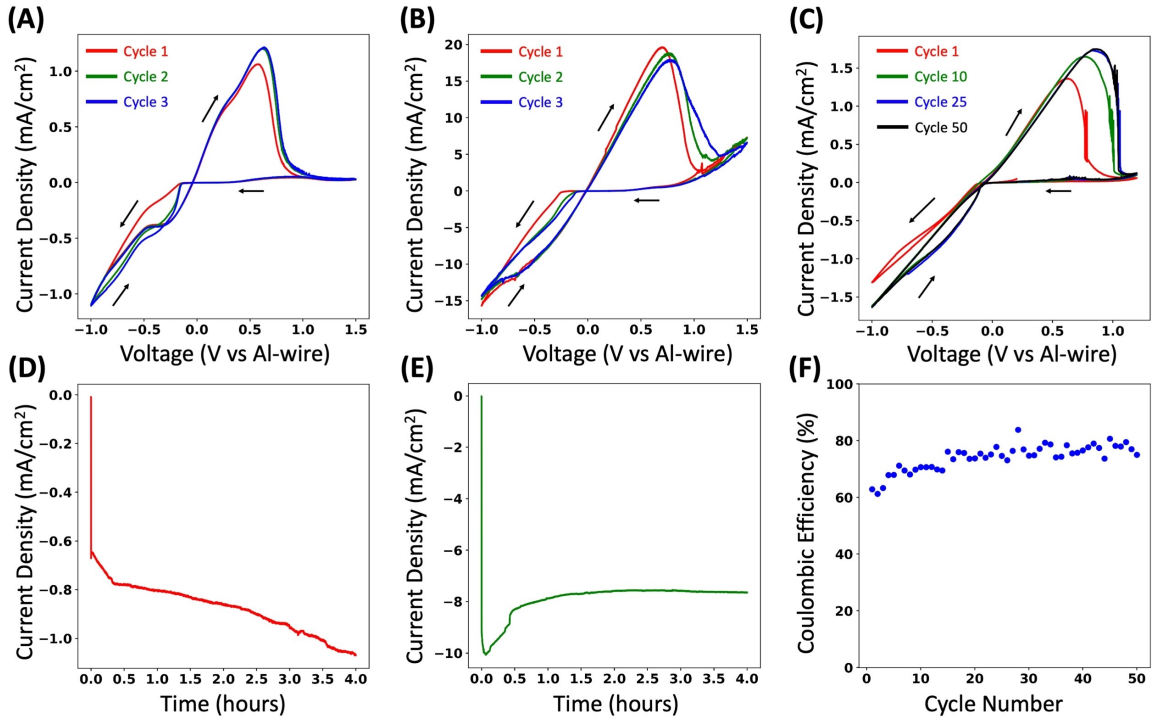

Figure 2. Cyclic voltammograms on gold working electrode at 50 mV/s of A) 1:3 $Al(OTF)_3$:$LiAlH_4$/THF, B) 1:3 $AlCl_3$:$LiAlH_4$/THF, and corresponding chronoamperograms on Cu substrate of D) 1:3 $Al(OTF)_3$:$LiAlH_4$/THF at −0.25 V (vs Al/Al^{3+}), and E) 1:3 $AlCl_3$:$LiAlH_4$/THF at −0.25 V (vs Al/Al^{3+}). C) Al plating/stripping cycling of 1:3 $Al(OTF)_3$:$LiAlH_4$/THF on gold working electrode at 50 mV/s and F) corresponding coulombic efficiencies.

Research Article
doi.org/10.1002/batt.202300164
Chemistry Europe
European Chemical Societies Publishing

Our hypothesis is that the H^- adsorb to the electrode surface enabling reversible Al plating in a process similar to that of the Cl^- in the magnesium aluminum chloride complex electrolytes.[77]

We speculate that the electrochemical mechanism in the OTF^--based electrolyte is analogous to that proposed for Ca plating from $Ca(BH_4)_2$/THF,[78] and that the production of free H^- and AlH_3 from AlH_4^- is catalyzed by metal substrates, both of which are essential for Al plating. This process is dictated by the equilibrium proposed in Reaction (3) and the AlH_3 species are electrochemically reduced to Al metal during the electrochemical reduction reaction. This, in turn, further increases the concentration of free H^- at the interface and allows for stripping of the plated Al, but also makes the electrolyte susceptible to a side reaction involving the oxidative generation of H_2 which leads to the growth in anodic charge and coulombic efficiency.

Plating and characterization of aluminum deposits

To confirm Al plating from both electrolytes, chronoamperometry, optical microscopy and scanning electron microscopy experiments were conducted. Plating of Al on a Cu substrate from both electrolytes was achieved by holding the potential at either −0.25 V (vs. Al/Al^{3+}) for 4 hours or −0.2 V (vs. Al/Al^{3+}) for 18 hours. (see Experimental Section for details) As was the case for the cyclic voltammetry experiments shown in Figure 2(A and B), the measured current densities during the chronoamperometry experiments in the Cl^--based electrolyte (Figure 2E) are one order of magnitude higher than that of the OTF^--based electrolytes (Figure 2D), re-enforcing the fact that the Cl^- significantly facilitate the plating process, as we have demonstrated in our previous report.[41] Given the similar concentrations and observed viscosities between the solutions, these results strongly suggest that the Cl^--based electrolyte is likely to have much higher nucleation densities than the OTF-based electrolyte.

Interestingly, a gradual increase in current density is observed only in the chronoamperogram of the OTF^--based electrolyte (Figure 2D), whereas a current plateau is recorded for the Cl^--based electrolyte. The increase in current densities during chronoamperometry experiments has been attributed to an increase in the electroactive surface area,[79,80] which in this case could be associated with the increase in the concentration of free H^- at the interfaces that occurs as a result of continuous Al plating.

The optical microscopy images and XRD patterns of the Al deposits from the OTF^--based and the Cl^--based electrolytes are shown in Figure 3. The overall effectiveness of the OTF^--based electrolyte for plating of Al is evident from the optical microscopy images Figure 3(A–D) and the photographic images in Figure S5(A and B). To verify that the grain-like deposits observed on the Cu substrate corresponds to crystalline Al, XRD spectra were compared to that of an untreated Cu substrate and an Al foil. Clearly, the Al deposits from both the OTF^--based and Cl^--based electrolytes exhibit a diffraction pattern which is identical to that of the Al foil.

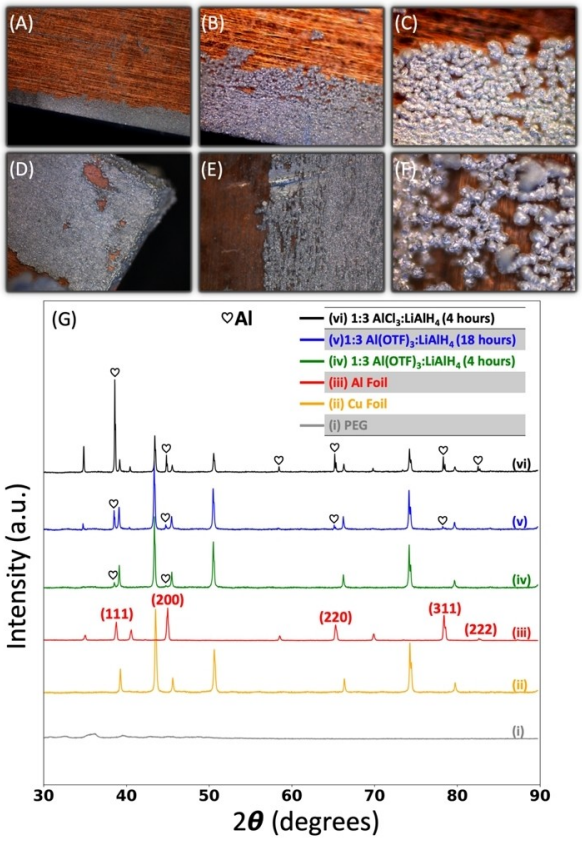

Figure 3. Optical microscopy images of Al electrodeposits on Cu substrate from 1:3 $Al(OTF)_3$:$LiAlH_4$/THF at −0.25 V (vs. Al/Al^{3+}) for 4 hours at magnification of A) 5×, B) 20×, C) 50×, and Al electrodeposits on Cu substrate after 18 hours at −0.2 V (vs. Al/Al^{3+}) from highly concentrated 1:3 $Al(OTF)_3$:$LiAlH_4$/THF electrolyte at magnification of D) 5× and from $AlCl_3$:$LiAlH_4$/THF at magnification of E) 5× and F) 20×. G) X-ray diffraction pattern of aluminum electrodeposits on Cu substrates.

The surface morphology of the Al deposits was further examined by a scanning electron microscope (SEM) and the results are displayed in Figure 4.

These results clearly reveal that Al plating can be carried out in the absence of any active-halide components (such as, $AlCl_2^+ \cdot n$THF, $AlCl_3 \cdot n$THF and $AlCl_4^-$ where n = number of coordinating THF) and that the electrochemical process in the OTF^--based electrolyte is entirely due to Al-hydride species. However, it should be noted that, although the OTF anions are chemically stable in solution, this does not necessarily mean that they are shielded from electrochemical decomposition which may occur during the plating process. This hypothesis could perhaps explain the presence of AlF_3 in the Al deposits as will be revealed in the following section.

Research Article
doi.org/10.1002/batt.202300164
Chemistry Europe
European Chemical Societies Publishing

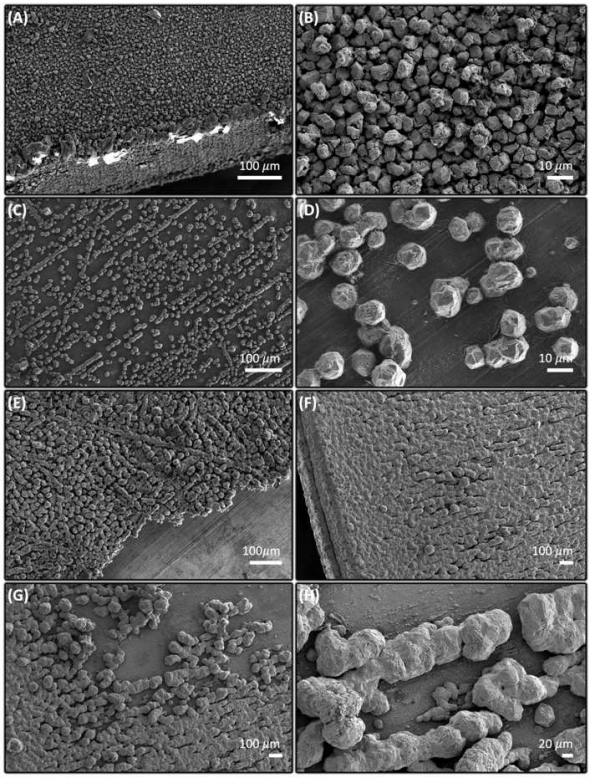

Figure 4. SEM micrographs of Al electrodeposits on Cu substrate from 1 : 3 $Al(OTF)_3$: $LiAlH_4$/THF after 4 hours at −0.25 V (vs. Al/Al^{3+}) at A), B) region 1, and C), D) region 2, and E) after 18 hours at −0.2 V (vs. Al/Al^{3+}) from highly concentrated 1 : 3 $Al(OTF)_3$: $LiAlH_4$/THF electrolyte, and from F–H) 1 : 3 $AlCl_3$: $LiAlH_4$/THF after 4 hours at −0.25 V (vs. Al/Al^{3+}).

Revealing chemical composition of the Al deposits via surface and depth-profile XPS and confirming electrochemical reversibility

To uncover the chemical composition of the electrodeposited Al films from the 4-hour chronoamperometry experiments, the Cu substrates were characterized by depth-profile XPS analysis, and the results are shown in Figure 5. The Al 2p spectra for the Al deposits obtained from the OTF^--based electrolytes shown in Figure 5(A), strongly indicates that Al metal, Al_2O_3, and AlF_3 are present. The peak at 72.8 eV is well-known to be associated with Al metal of an Al-foil.[81] In the case of Al plating from organic electrolytes, however, it is worth mentioning that this peak has only been reported as a fitting of a broad peak at ca. 74 eV, involving both Al and Al_2O_3 on Al.[40] Here, for the first time, clear peak separation is observed in our XPS data, as shown in Figure 5(A). As for the peak associated with AlF_3 (ca. 78 eV), this peak was previously reported at 77.0 eV by Wen et al for the Al deposits obtained from $Al(PF_6)_3$/DMSO.[40]

Upon etching the thin Al film with argon for 5 minutes, the peak attributed to the Al-metal at 72.8 eV remains unchanged, while the peaks attributed to Al_2O_3 and AlF_3 became more prominent. Also, the AlF_3 peak becomes broader due to the contribution from the Cu 3p at ca. 80 eV. A clear distinction between the peaks of the Al 2p of AlF_3 (at ca. 78 eV) and the Cu 3p (at ca. 80 eV) of the Cu substrate, in addition to the peaks associated with organic- and metallic-fluorine[82] was made by examining another region of the electrode surface (region 2), where the surface coverage of Al on Cu is significantly lower than that of region 1. A comparison of the XPS spectra of the two regions is shown in Figure S6. Additionally, before etching, a weak-intensity peak is observed at 933 eV in the Cu 2p spectrum. After etching, the relative intensity of this peak increases along with the appearance of a peak at 952.8 eV, indicating that a significant portion of the Al film has been completely removed exposing the Cu substrate. To experimentally confirm this result, after completing the XPS experiment, the Cu substrate was re-examined by a SEM and the result revealing the residual Al on Cu is shown Figure S7.

In contrast, the Al 2p spectra of the etched and unetched Al film obtained from the Cl^--based electrolyte shown in Figure 5(D) suggests that the film is primarily comprised of Al_2O_3 and an aluminum chloride (Al_xCl_y) contaminant. The presence of the Al_xCl_y contaminant can be inferred from the Cl 2p spectra (Figure 5E) which reveals a peak in the 199–204 eV region suggesting the presence of both organic and metallic (Al–Cl) chloride components.[83] Examining another region of the electrode, a small, yet significant peak at 72.8 eV associated with metallic Al is observed as shown in spectrum (*v*) in Figure S6. In addition to the reactivity of the Al film with the electrolyte components during the plating process, the high degree of oxide- and chloride-components of the Al film can be attributed to the participation of $AlX_3(THF)_n$ (where X is Cl or H, and $n = 0$, 1 or 2) species in the plating process. Furthermore, the Cl 2p peak persists even after etching as shown in Figure 5(E), confirming that Cl^- is not only found as a surface contaminant, but also within the Al film. It is worth mentioning that the presence of Cl^- contaminants is not unusual, but rather expected for $AlCl_3$-based electrolytes, as it has also been reported for $AlCl_3$/diglyme electrolytes.[61]

Lastly, to validate that the plating process is in fact reversible, additional chronoamperometry experiments were carried out. For comparison purposes, initially, Al plating was carried out on a Cu substrate by holding the potential for 1 hour at −0.25 V (vs. Al/Al^{3+}). A current plateau is observed throughout the entire process as shown in Figure 6(A). The Cu substrate was then examined, and Al plating was confirmed by optical microscopy and SEM as shown in Figure 6(B and C) (see also Figure S10). Another sample was prepared using the same method, this time however, the potential was switched at the 1-hour mark to +0.25 V (vs. Al/Al^{3+}) and held for an additional 1 hour. The chronoamperogram associated with this process is shown in Figure 6(D). From the chronoamperogram in Figure 6(D), the ratio of anodic to cathodic charge was calculated and found to be 67.8%, implying approximately 32% of the deposited aluminum remained behind, likely due to the presence of Al_2O_3 and AlF_3 in the deposit that was observed via depth-profile XPS analyses, preventing complete stripping of the as-deposited material. Following the chronoamperometry experiment, the Cu substrate was examined to confirm that the stripping process was successful. Indeed, very few Al deposits remained on the Cu substrate as shown in Figure 6(E and F) (see also Figure S11).

Research Article
doi.org/10.1002/batt.202300164
Chemistry Europe
European Chemical Societies Publishing

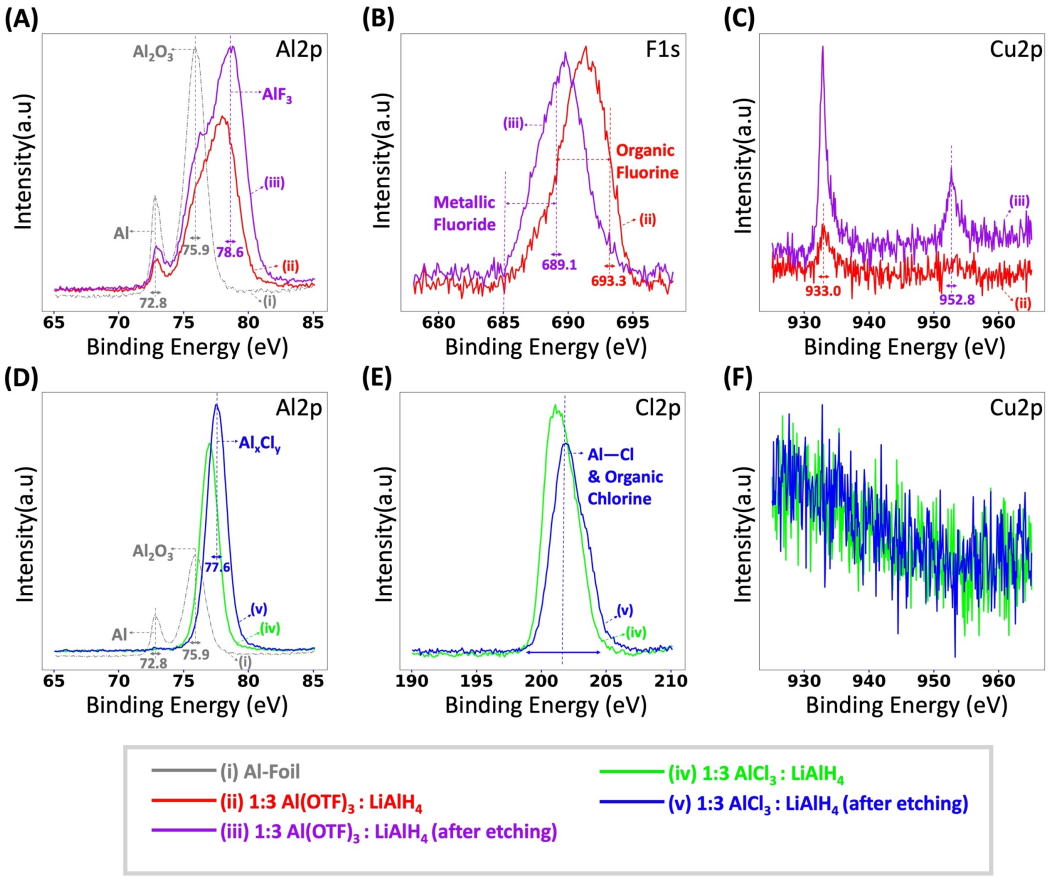

Figure 5. XPS spectra for aluminum electrodeposits (region 1) from A–C) 1 : 3 $Al(OTF)_3$: $LiAlH_4$/THF, and Al electrodeposits (region 1) from D–F) 1 : 3 $AlCl_3$: $LiAlH_4$/THF.

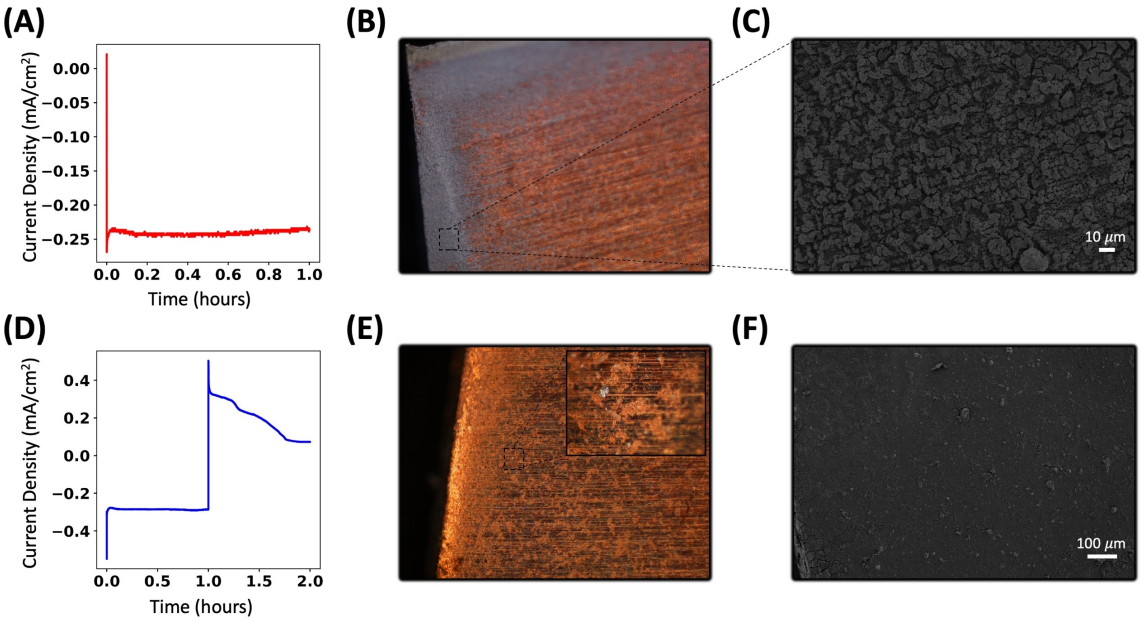

Figure 6. Chronoamperogram of A) Al plating on Cu substrate from 1 : 3 $Al(OTF)_3$: $LiAlH_4$/THF at −0.25 V (vs. Al/Al^{3+}) for 1-hour and corresponding B) optical microscopy at 5× magnification and C) SEM images. Chronoamperogram of D) Al plating followed by stripping on Cu substrate from 1 : 3 $Al(OTF)_3$: $LiAlH_4$/THF at −0.25 V and +0.25 V (vs. Al/Al^{3+}), respectively, and corresponding E) optical microscopy at 5× magnification (100× for inset) and F) SEM images.

Conclusions

The results in this report indicate potential application of an active-halide-free (AHF) organic electrolyte in rechargeable Al batteries. By introducing a $LiAlH_4$ additive to an $Al(OTF)_3$/THF electrolyte, we have demonstrated that the H^- play an integral role in plating/stripping Al in organic electrolytes, allowing the process to occur in the absence of any active-halide species (such as, $AlCl_2^+ \cdot n$THF, $AlCl_3 \cdot n$THF, and $AlCl_4^-$ where n = number of coordinating THF). Al deposits, although visually evident on the Cu substrates, were also confirmed by several characterization techniques including optical microscopy, SEM, XRD and XPS. XPS etching experiments confirm that significant reactivity occurs between the freshly-plated Al and the electrolyte components as evident by the F- and Cl-XPS spectra from the OTF^-- and Cl^--based electrolytes, respectively. Results from DFT and FTIR have shown that the strategy employed to evaluate the hydride additive by relying on the spectroscopic attributes of the OTF^-, can allow for the evaluation of other Li-based additives not just LiCl as we have previously demonstrated.[41]

Outlook

While the work demonstrated in this report overcomes a milestone in organic electrolyte development for rechargeable Al batteries, much work is still needed. In addition to evaluating this electrolyte with several cathode materials, perhaps those less prone to hydride reactivity, studying the reaction in other organic solvents will be necessary. Ideally, the choice of the organic solvent should be limited to those compatible with $LiAlH_4$. For instance, our preliminary cyclic voltammetry evaluation of an electrolyte consisting of $Al(OTF)_3$ and $LiAlH_4$ in diglyme reveals a reversible electrochemical process ca. 0 V (vs. Al/Al^{3+}), likely associated with reversible Al plating and stripping, as shown in Figure S12. Although more flammable than THF, dimethyl ether is also well known to dissolve $LiAlH_4$ and may be considered a suitable candidate.[42] We speculate that borohydrides (BH_4^-) can have similar effect on the plating and stripping behavior of Al-ions, especially because of the critical role BH_4^- play in magnesium[84] and calcium[78,85,86] electrolyte chemistries. Future work will focus on evaluating the role of $LiBH_4$ on the $Al(OTF)_3$/THF electrolytes. We also speculate that a similar plating/stripping behavior can occur in the absence of the fluoride-component, this hypothesis will be explored by replacing the $Al(OTF)_3$ salt with a halide-free and THF-soluble Al salts. Lastly, while FTIR and DFT calculation for ionic species present in solution provide interesting insight into chemical speciation and help understand possible dissociation and electrochemical mechanisms, a more detailed investigation of the OTF^--based electrolyte using Nuclear Magnetic Resonance (NMR) spectroscopy, Mass Spectrometry (MS), and Electrochemical Quartz Crystal Microbalance (EQCM) is necessary.

Supporting Information

Measured and computed vibrational frequencies of Al complexes. Timeline of Al organic electrolytes. Calculated Al–H bond lengths in $Al_2H_7^-$ and $Al_2Cl_3H_4^-$. Additional CVs, photographic images, optical microscopy, and SEM images of Al plating/stripping. XPS data for 2 regions on Cu substrate. SEM images of Cu substrate after etching from OTF^--based electrolyte.

Author Contributions

Z. S: Conceptualization, Methodology, Data Curation, Formal analysis, Investigation, Software, Visualization, Writing – original draft, review & editing. E. J. M: Conceptualization, Funding acquisition, Methodology, Project administration, Resources, Supervision, Validation, Writing – review & editing.

Acknowledgements

The authors acknowledge computing time on Multi-Environment Computer for Exploration and Discovery (MERCED) Cluster which is supported by National Science Foundation Grant no. ACI-1429783. Scanning electron microscopy (SEM), X-ray diffraction (XRD), and X-ray photoelectron spectroscopy (XPS) resources were provided by Imaging and Microscopy Facility (IMF) at UC Merced. Z. S thanks Kennedy Nguyen for technical assistance with the SEM, XRD and XPS instrumentation. The computations requested during the peer-review of this work (i.e., binding energies) were enabled by resources provided by the National Academic Infrastructure for Supercomputing in Sweden (NAISS) at Tetralith partially funded by the Swedish Research Council through grant agreement no. 2022-06725.

Conflict of Interests

The authors declare no conflict of interest.

Data Availability Statement

The data that support the findings of this study are available from the corresponding author upon reasonable request.

Keywords: electrodeposition · room-temperature · electrolytes · chloride-free · Al-ion

[1] J. B. Goodenough, *Energy Storage Mater.* **2015**, *1*, 158–161.
[2] M. Li, J. Lu, Z. Chen, K. Amine, *Adv. Mater.* **2018**, *30*, 1800561.
[3] X. Zeng, M. Li, D. Abd El-Hady, W. Alshitari, A. S. Al-Bogami, J. Lu, K. Amine, *Adv. Energy Mater.* **2019**, *9*, 1900161.
[4] M. Li, J. Lu, X. Ji, Y. Li, Y. Shao, Z. Chen, C. Zhong, K. Amine, *Nat. Rev. Mater.* **2020**, *5*, 276–294.
[5] Y. Liang, H. Dong, D. Aurbach, Y. Yao, *Nat. Energy* **2020**, *5*, 646–656.

[6] J. Tu, W.-L. Song, H. Lei, Z. Yu, L.-L. Chen, M. Wang, S. Jiao, *Chem. Rev.* **2021**, *121*, 4903–4961.
[7] G. A. Elia, K. Marquardt, K. Hoeppner, S. Fantini, R. Lin, E. Knipping, W. Peters, J.-F. Drillet, S. Passerini, R. Hahn, *Adv. Mater.* **2016**, *28*, 7564–7579.
[8] G. A. Elia, K. V. Kravchyk, M. V. Kovalenko, J. Chacón, A. Holland, R. G. Wills, *J. Power Sources* **2021**, *481*, 228870.
[9] P. R. Gifford, J. B. Palmisano, *J. Electrochem. Soc.* **1988**, *135*, 650.
[10] N. Jayaprakash, S. K. Das, L. A. Archer, *Chem. Commun.* **2011**, *47*, 12610–12612.
[11] L. D. Reed, E. Menke, *J. Electrochem. Soc.* **2013**, *160*, A915-A917.
[12] L. Geng, G. Lv, X. Xing, J. Guo, *Chem. Mater.* **2015**, *27*, 4926–4929.
[13] H. Wang, Y. Bai, S. Chen, X. Luo, C. Wu, F. Wu, J. Lu, K. Amine, *ACS Appl. Mater. Interfaces* **2015**, *7*, 80–84.
[14] M.-C. Lin, M. Gong, B. Lu, Y. Wu, D.-Y. Wang, M. Guan, M. Angell, C. Chen, J. Yang, B.-J. Hwang, *Nature* **2015**, *520*, 324–328.
[15] N. P. Stadie, S. Wang, K. V. Kravchyk, M. V. Kovalenko, *ACS Nano* **2017**, *11*, 1911–1919.
[16] G. A. Elia, I. Hasa, G. Greco, T. Diemant, K. Marquardt, K. Hoeppner, R. J. Behm, A. Hoell, S. Passerini, R. Hahn, *J. Mater. Chem. A* **2017**, *5*, 9682–9690.
[17] M. Walter, K. V. Kravchyk, C. Böfer, R. Widmer, M. V. Kovalenko, *Adv. Mater.* **2018**, *30*, 1705644.
[18] H. Chen, H. Xu, S. Wang, T. Huang, J. Xi, S. Cai, F. Guo, Z. Xu, W. Gao, C. Gao, *Sci. Adv.* **2017**, *3*, eaao7233.
[19] X. Wen, Y. Liu, A. Jadhav, J. Zhang, D. Borchardt, J. Shi, B. M. Wong, B. Sanyal, R. J. Messinger, J. Guo, *Chem. Mater.* **2019**, *31*, 7238–7247.
[20] H. Yang, H. Li, J. Li, Z. Sun, K. He, H.-M. Cheng, F. Li, *Angew. Chem. Int. Ed.* **2019**, *58*, 11978–11996.
[21] Q.-X. Qin, M. Skyllas-Kazacos, *J. Electroanal. Chem. Interfacial Electrochem.* **1984**, *168*, 193–206.
[22] R. J. Gale, R. A. Osteryoung, *Inorg. Chem.* **1979**, *18*, 1603–1605.
[23] J. Shi, J. Zhang, J. Guo, *ACS Energy Lett.* **2019**, *4*, 2124–2129.
[24] C.-H. Tseng, J.-K. Chang, J.-R. Chen, W. T. Tsai, M.-J. Deng, I.-W. Sun, *Electrochem. Commun.* **2010**, *12*, 1091–1094.
[25] H. Wang, S. Gu, Y. Bai, S. Chen, N. Zhu, C. Wu, F. Wu, *J. Mater. Chem. A* **2015**, *3*, 22677–22686.
[26] P. K. Lai, M. Skyllas-Kazacos, *J. Electroanal. Chem.* **1988**, *248*, 431–440.
[27] R. T. Carlin, W. Crawford, M. Bersch, *J. Electrochem. Soc.* **1992**, *139*, 2720.
[28] R. Jay, A. W. Tomich, J. Zhang, Y. Zhao, A. De Gorostiza, V. Lavallo, J. Guo, *ACS Appl. Mater. Interfaces* **2019**, *11*, 11414–11420.
[29] R. D. Howells, J. D. Mc Cown, *Chem. Rev.* **1977**, *77*, 69–92.
[30] Y. Yang, W. Wang, Y. Nuli, J. Yang, J. Wang, *ACS Appl. Mater. Interfaces* **2019**, *11*, 9062–9072.
[31] D. Huang, S. Tan, M. Li, D. Wang, C. Han, Q. An, L. Mai, *ACS Appl. Mater. Interfaces* **2020**, *12*, 17474–17480.
[32] E. Sheha, M. Farrag, S. Fan, E. Kamar, N. Sa, *ACS Appl. Energ. Mater.* **2022**, *5*, 2260–2269.
[33] L. D. Reed, S. N. Ortiz, M. Xiong, E. J. Menke, *Chem. Commun.* **2015**, *51*, 14397–14400.
[34] H. Wang, S. Gu, Y. Bai, S. Chen, F. Wu, C. Wu, *ACS Appl. Mater. Interfaces* **2016**, *8*, 27444–27448.
[35] L. D. Reed, A. Arteaga, E. J. Menke, *J. Phys. Chem. B* **2015**, *119*, 12677–12681.
[36] T. Mandai, P. Johansson, *J. Mater. Chem. A* **2015**, *3*, 12230–12239.
[37] T. Mandai, P. Johansson, *J. Phys. Chem. C* **2016**, *120*, 21285–21292.
[38] M. Chiku, S. Matsumura, H. Takeda, E. Higuchi, H. Inoue, *J. Electrochem. Soc.* **2017**, *164*, A1841.
[39] Z. Slim, E. J. Menke, *J. Phys. Chem. B* **2020**, *124*, 5002–5008.
[40] X. Wen, J. Zhang, H. Luo, J. Shi, C. Tsay, H. Jiang, Y.-H. Lin, M. A. Schroeder, K. Xu, J. Guo, *J. Phys. Chem. Lett.* **2021**, *12*, 5903–5908.
[41] Z. Slim, E. J. Menke, *J. Phys. Chem. C* **2022**, *126*, 2365–2373.
[42] D. E. Couch, A. Brenner, *J. Electrochem. Soc.* **1952**, *99*, 234.
[43] G. A. Capuano, W. G. Davenport, *J. Electrochem. Soc.* **1971**, *118*, 1688.
[44] T. Hisano, T. Terazawa, I. Takeuchi, S. Inohara, H. Ikeda, *Bull. Chem. Soc. Jpn.* **1971**, *44*, 599–603.
[45] N. Ishibashi, M. Yoshio, *Electrochim. Acta* **1972**, *17*, 1343–1352.
[46] M. Yoshio, N. Ishibashi, *J. Appl. Electrochem.* **1973**, *3*, 321–325.
[47] E. Peled, E. Gileadi, *J. Electrochem. Soc.* **1976**, *123*, 15.
[48] M. Galová, *Chem. Pap.* **1982**, *36*, 791–797.
[49] M. W. M. Graef, *J. Electrochem. Soc.* **1985**, *132*, 1038.
[50] W. A. Badawy, B. A. Sabrah, N. H. Y. Hilal, *J. Appl. Electrochem.* **1987**, *17*, 357–369.
[51] L. Legrand, A. Tranchant, R. Messina, *J. Electrochem. Soc.* **1994**, *141*, 378.
[52] L. Legrand, A. Tranchant, R. Messina, *Electrochim. Acta* **1994**, *39*, 1427–1431.
[53] L. Legrand, M. Heintz, A. Tranchant, R. Messina, *Electrochim. Acta* **1995**, *40*, 1711–1716.
[54] L. Legrand, A. Tranchant, R. Messina, *Electrochim. Acta* **1996**, *41*, 2715–2720.
[55] M. C. Lefebvre, B. E. Conway, *J. Electroanal. Chem.* **1998**, *448*, 217–227.
[56] M. C. Lefebvre, B. E. Conway, *J. Electroanal. Chem.* **2000**, *480*, 34–45.
[57] M. C. Lefebvre, B. E. Conway, *J. Electroanal. Chem.* **2000**, *480*, 46–58.
[58] A. Kitada, K. Nakamura, K. Fukami, K. Murase, *Electrochemistry* **2014**, *82*, 946–948.
[59] Y. Nakayama, Y. Senda, H. Kawasaki, N. Koshitani, S. Hosoi, Y. Kudo, H. Morioka, M. Nagamine, *Phys. Chem. Chem. Phys.* **2015**, *17*, 5758–5766.
[60] M. Miyake, H. Fujii, T. Hirato, *Surf. Coat. Technol.* **2015**, *277*, 160–164.
[61] A. Kitada, K. Nakamura, K. Fukami, K. Murase, *Electrochim. Acta* **2016**, *211*, 561–567.
[62] A. Kitada, Y. Kato, K. Fukami, K. Murase, *Journal of The Surface Finishing Society of Japan* **2018**, *69*, 310–311.
[63] B. Zhang, Z. Shi, L. Shen, A. Liu, J. Xu, X. Hu, *J. Electrochem. Soc.* **2018**, *165*, D321.
[64] N. Yitzhack, P. Tereschuk, N. Sezin, D. Starosvetsky, A. Natan, Y. Ein-Eli, *J. Solid State Electrochem.* **2020**, *24*, 2833–2846.
[65] X. Wen, Y. Liu, D. Xu, Y. Zhao, R. K. Lake, J. Guo, *J. Phys. Chem. Lett.* **2020**, *11*, 1589–1593.
[66] Z. Zhang, A. Kitada, S. Gao, K. Fukami, N. Tsuji, Z. Yao, K. Murase, *ACS Appl. Mater. Interfaces* **2020**, *12*, 43289–43298.
[67] W. Peters, H. T. Duong, S. Lee, J.-F. Drillet, *Phys. Chem. Chem. Phys.* **2021**, *23*, 21923–21933.
[68] T. E. G. Daenen, *Nature* **1979**, *280*, 378–380.
[69] M. J. Frisch, G. W. Trucks, H. B. Schlegel, G. E. Scuseria, M. A. Robb, J. R. Cheeseman, G. Scalmani, V. Barone, B. Mennucci, G. A. Petersson, **2009**.
[70] A. D. Becke, *J. Chem. Phys.* **1993**, *98*, 5648–5652.
[71] R. Krishnan, J. S. Binkley, R. Seeger, J. A. Pople, *J. Chem. Phys.* **1980**, *72*, 650–654.
[72] R. Frech, W. Huang, *J. Solution Chem.* **1994**, *23*, 469–481.
[73] W. Huang, R. Frech, R. A. Wheeler, *J. Phys. Chem.* **1994**, *98*, 100–110.
[74] J. Derouault, P. Granger, M. T. Forel, *Inorg. Chem.* **1977**, *16*, 3214–3218.
[75] V. A. Yartys, R. V. Denys, J. P. Maehlen, C. Frommen, M. Fichtner, B. M. Bulychev, H. Emerich, *Inorg. Chem.* **2007**, *46*, 1051–1055.
[76] A. E. Finholt, A. C. Bond Jr, H. I. Schlesinger, *J. Am. Chem. Soc.* **1947**, *69*, 1199–1203.
[77] K. A. See, K. W. Chapman, L. Zhu, K. M. Wiaderek, O. J. Borkiewicz, C. J. Barile, P. J. Chupas, A. A. Gewirth, *J. Am. Chem. Soc.* **2016**, *138*, 328–337.
[78] K. Ta, R. Zhang, M. Shin, R. T. Rooney, E. K. Neumann, A. A. Gewirth, *ACS Appl. Mater. Interfaces* **2019**, *11*, 21536–21542.
[79] J. Pavlovski, S. Myrskog, P. Dufour, C. M. Gabardo, L. Soleymani, *J. Electrochem. Soc.* **2015**, *162*, D503.
[80] Y. T. Jee, M. Park, S. Cho, J.-I. Yun, *Sci. Rep.* **2019**, *9*, 1–10.
[81] Y. L. Yan, M. A. Helfand, C. R. Clayton, *Appl. Surf. Sci.* **1989**, *37*, 395–405.
[82] T. Onodera, T. Nakakawaji, K. Adachi, K. Kurihara, M. Kubo, *J. Phys. Chem. C* **2016**, *120*, 10857–10865.
[83] N. Canever, F. R. Hughson, T. Nann, *ACS Appl. Energ. Mater.* **2020**, *3*, 3673–3683.
[84] R. Mohtadi, M. Matsui, T. S. Arthur, S.-J. Hwang, *Angew. Chem.* **2012**, *124*, 9918–9921.
[85] D. Wang, X. Gao, Y. Chen, L. Jin, C. Kuss, P. G. Bruce, *Nat. Mater.* **2018**, *17*, 16–20.
[86] A. M. Melemed, D. A. Skiba, B. M. Gallant, *J. Phys. Chem. C* **2022**, *126*, 892–902.

Manuscript received: April 18, 2023
Revised manuscript received: June 4, 2023
Accepted manuscript online: June 19, 2023
Version of record online: July 20, 2023